A First Principal investigation for Structural, Electronic and Mechanical Properties of α-Mg_3N_2

M C Rolania[a], and G Sharma

Department of Pure & Applied Physics, University of Kota, Kota-324005, India.

mangalrolania@gmail.com

Abstract

In this present work, the LCAO technique is employed to explore the structural, mechanical, as well as electronic characteristics of the α-Mg_3N_2 material. The study utilizes the GGA approach within the framework of Density Functional Theory (DFT) to optimize geometrical parameters and characterize the material's structural attributes. The findings indicate that α-Mg_3N_2 demonstrates semiconducting behaviour, as inferred from its electronic properties. With an energy band gap aligning with the optimal range of the solar spectrum, α-Mg_3N_2 is identified as a potential candidate for photovoltaic applications. A comprehensive analysis of elastic properties, including bulk modulus, shear modulus, Young's modulus, with Poisson's ratio, was discussed. Additionally, the anisotropic nature of Young's modulus, linear compressibility has been evaluated via ELATE software, revealing the predetermined elastic anisotropy of the α-Mg_3N_2 compound. Hence, the results of this investigation indicate that α-Mg_3N_2 is a good candidate for the photovoltaic sector.

Keywords: Semiconductor, Electronic structure, LCAO method, Band structure, Elastic properties.
Received 28 January 2025; First Review 11 February 2025; Accepted 19 March 2025.

*** Address of correspondence**
M C Rolania
Department of Pure & Applied Physics,
University of Kota, Kota-324005, India

Email: mangalrolania@gmail.com

How to cite this article
M C Rolania, and G Sharma, A First Principal investigation for Structural, Electronic and Mechanical Properties of α-Mg_3N_2, J. Cond. Matt. 2025; 03 (01): 84-90.

Available from:
https://doi.org/10.61343/jcm.v3i01.83

Introduction

Binary nitrides with II group elements (M_3N_2, where M = Be, Mg, Ca, Sr, Ba), have been studied for over a century [1] and are utilized across various scientific and industrial domains. These compounds serve as precursors in the synthesis of complex nitrides [2]. In industrial applications, they play diverse roles, including acting as additives in steel refinement processes [3], as additive for densification of aluminum nitride (AlN) along with silicon nitride (Si_3N_4) [4], and as catalysts facilitating the transformation of hexagonal phase of boron nitride (h-BN) in the cubic form (c-BN) [5]. Furthermore, Be_3N_2 and Mg_3N_2 have been explored in conjunction with lithium–nitrogen materials (e.g., LiN_3 and Li_2NH) for potential applications in hydrogen storage [6]. The investigation of novel semiconductors necessitates the fabrication of materials with exceptional purity to guarantee that the assessment of intrinsic physical characteristics, such as lattice constants, effective electron mass, or energy gap, is not influenced by defects. A representative case is indium nitride (InN), with energy gap is assumed to be approximately 1.9 eV for many years [7]. However, with the ease of use of premium samples in the early 2000s [8, 9], the accurate measurement of its band gap revealed a value of around 0.7 eV. A similar scenario is observed with magnesium nitride (Mg_3N_2). This is particularly intriguing, specified that its anti-bixbyite crystal arrangement and lattice components are initially determined using powder form samples and millimeter-scale single crystals at earliest [10], with further refinement carried out [11].

Ceramic magnesium nitride (Mg_3N_2) has been extensively utilized in industrial applications the same as nitriding representative to facilitate the synthesis of diverse nitride compounds [12, 13] and as a catalyst in the production of ultra-hard materials such as silicon nitride with cubic phase boron nitride [14]. In recent developments, Mg_3N_2 has also demonstrated potential in advanced applications, including high-thermal-conductivity ceramics when alloyed amid silicon [15] and as a reversible medium for hydrogen storage [16]. Notably, these uses predominantly capitalize on the material's physicochemical attributes, with little attention given to its optoelectronic characteristics. Limited theoretical studies on crystalline Mg_3N_2 suggest that it behaves as a semiconductor, exhibiting an energy band gap ranging from 1.1 to 2.26 eV, depending upon the computational approach employed [17]. Current

discussions have primarily focused on its crystal structure and the other properties of α-Mg_3N_2 through ab initio methodologies [18, 19]. Limited computational studies have analyzed its electronic properties; however, reported values for the electronic band gap (E_g) vary significantly, ranging from 1.133 to 1.19 eV [20, 21]. For a material to be viable in the PV industry, it is essential to determine its structural, electronic and mechanical properties.

Computational Details

An ab initio study of α-Mg_3N_2 is conducted using the Linear Combination of Atomic Orbitals (LCAO) methodology embodied in the CRYSTAL software package [22, 23]. After expanding atomic orbitals into linear combinations of Bloch functions using localized basis sets, the method solves self-consistent Kohn-Sham (KS) equations. The all-electron Gaussian-type basis sets for Mg and N were taken from www.tcm.cam.ac.uk, to acquire a stable system [24, 25]. The proper coupling of electron-electron and electron-nucleus interactions is crucial for controlling computation accuracy. Therefore, a precise evaluation of the contributions of the Coulomb and Hartree-Fock (HF) exchanges to the Fock matrix and total energy is crucial. If the exchange parameter and Coulomb overlap are below the threshold, the corresponding bioelectronics integral was not taken into account during computation. For the computations of geometry optimization, frequency calculations, and elastic characteristics, the convergence criteria were maintained constant.

Structural optimization was carried out starting from the initial geometry, yielding optimized lattice parameters and fractional atomic coordinates. For these calculations, the PBE [26, 27] functional was utilized. The performance of above schemes is claimed to be better than other exchange-correlation potentials as it improves the equilibrium properties of solids and surfaces. These are very strong and commonly used functional for a variety of DFT applications because these potentials are very helpful in predictions of structures, formation energies, and general characteristics [26, 27]. The Monkhorst-Pack approach is used to sample reciprocal space, using 8×8×8 k-points that correspond to 35 k-vectors in the irreducible Brillouin zone. The self-consistent field (SCF) convergence criterion (TOLDEE) was set to 10^{-8}, and the Brillouin zone (Bz) was sampled using an 8 × 8 × 8 Monkhorst-Pack k-point grid [28], corresponding to 35 k-points of the irreducible Bz. Additionally, the BROYDEN mixing algorithm [29, 30] was applied to ensure robust convergence. The structural analysis began with the use of experimental parameters [31] to calculate the equilibrium volume (V_0). A full structural optimization, encompassing both lattice constants and atomic positions, was performed to determine V_0. Subsequently, the lattice energy was computed by introducing a ±8% variation in V_0, and the resulting data were fitted via an equation of state (EOS) algorithm [32]. With the optimized structure, the electronic properties were subsequently evaluated.

Results and Discussions

Structural properties

At standard environment, magnesium nitride (Mg_3N_2) structured in a cubic lattice with the space group $Ia\bar{3}$ (No 206), adopting an anti-bixbyite-like structural arrangement. The unit cell comprises 16 formula units, amounting to a total of 80 atoms (48 magnesium and 32 nitrogen) in its typical crystallographic configuration. Nitrogen atoms occupy two distinct Wyckoff positions: 8b (N1) and 24d (N2), whereas magnesium atoms are situated at the 48e Wyckoff position. At equilibrium volume, the conventional and primitive cells of Mg_3N_2 are illustrated in Figure 1. The structural configuration reveals that nitrogen atoms form octahedral coordination with magnesium atoms, which are, in turn, tetrahedral coordinated by nitrogen atoms. Within the tetrahedral symmetry, each magnesium atom is bounded by one N1 atom along with three N2 atoms, with the bond lengths differing among them. The atomic environment of nitrogen differs due to its occupancy of two inequivalent crystallographic sites.

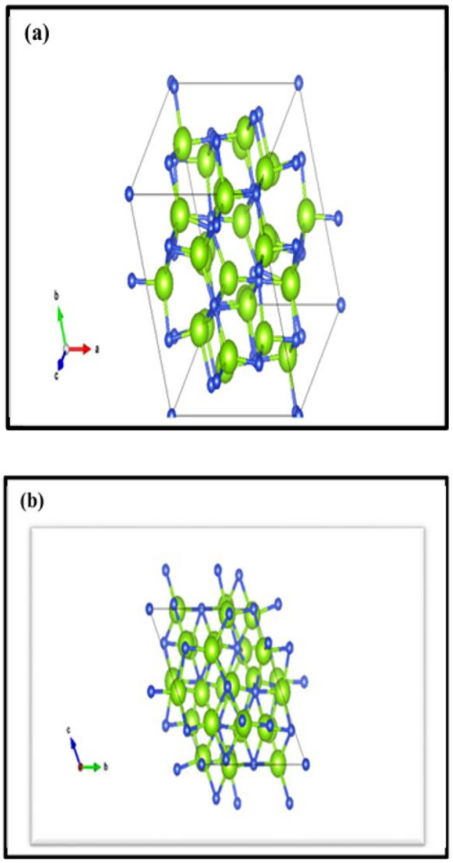

Figure 1: Structural arrangement of unit cells for α-Mg_3N_2.

To delve deeper into the analysis, the researchers aimed to simplify the structure of each material to identify its equilibrium lattice parameters corresponding to the most stable state. The energy variation as a function of volume is computed using the GGA exchange-correlation functionals. Subsequently, the data is fitted with the Birch–Murnaghan's EOS. The resulting energy-volume curve for the compounds is presented in Fig.2, with the derived parameters summarized in Table 1.

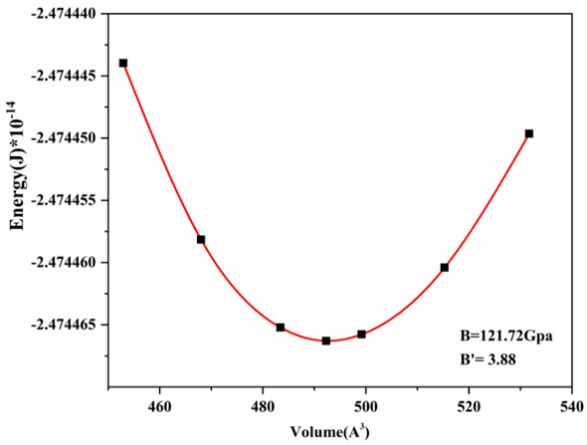

Figure 2: Volume optimization curve of α-Mg_3N_2.

Electronic properties

The appropriate assessment of electronic band gap energy is now the biggest problem because of its importance in the field of PV applications; even though the best potential for additional study has not been selected yet. The direct band gap value of Mg_3N_2 is determined to be 1.72 eV. As illustrated in Figure 3, the investigated materials display a conduction band minimum (CBM) and valence band maximum (VBM) that do not overlap, both situated at the high-symmetry Γ-point within the first Brillouin zone. Therefore, it can be concluded such compounds possess a direct band gap. Further, as we move along the directions Γ-P and Γ-H, it is observed that available energy states are decreasing and getting sharper in the second case, which shows the considerable difference. This characteristic signifies that the materials under study are categorized as direct band gap semiconductors and thus a possible candidate for PV applications. The band gap at the Γ point is near 1.72 eV in agreement with the earlier reported experimental and theoretical results. The computed band gap values correspond to approximately 62% of the experimentally determined value. It is widely recognized that DFT-GGA calculations typically underestimate the band gap in semiconductors and insulators, often predicting only 30% to 80% of the experimental value. This discrepancy arises due to the absence of integer discontinuities in the derivative of the exchange-correlation energy [34]. The results indicate the superior potential of the investigated material for optoelectronic applications, along with enhanced electron transitions from the valence band to the conduction band. The horizontal dashed line represents the reference energy level, denoting the Fermi level (EF).

The density of states (DOS), both total (TDOS) and partial (PDOS), of the investigated compound is computed to verify their semiconducting nature, as illustrated in Figure 4. The analysis discloses that the valence band (VB) is predominantly influenced by the contribution of the p-states of Mg and N atoms. The overlapping of energy bands between the energy ranges of -3 to -1 eV arises due to hybridizations between the s and p orbitals of Mg and N atoms, respectively. A lesser but still important part of the creation of this group of bands is played by the s-orbitals of two non-equivalent N atoms. The higher valence band is formed in part by the hybridized p-orbitals of the Mg and N atoms. It is believed that the band gap results from an electronic transition between the s-orbitals of Mg atoms and the s- and d-orbitals of N atoms. A secondary contribution to the VB arises from the d-orbitals of Mg atoms, with a minor input from the d-orbitals of the N2 atom, whereas the involvement of the N1 atom in the VB is negligible. Conversely, the conduction band (CB) is primarily composed of contributions from the Mg atom, while the roles of the N1 and N2 atoms in forming the conduction band are minimal.

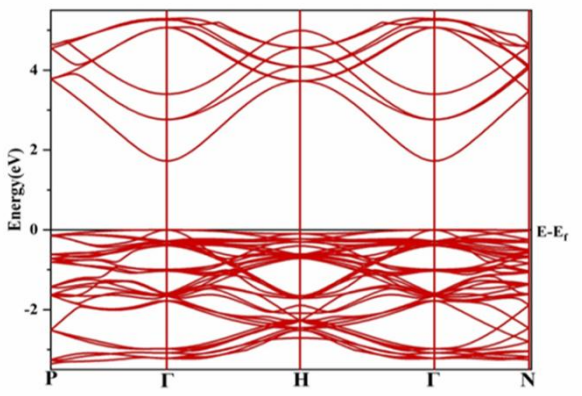

Figure 3: The band structures along the high-symmetry paths in the Brillouin zone (BZ) for α-Mg_3N_2 computed using the LCAO method. The Fermi energy, EF, represented by the horizontal line, has been aligned to the zero-energy reference level

Through a detailed examination of the PDOS for the studied materials, the orbital contributions of Mg and the N1 and N2 atoms to the TDOS near the Fermi level were identified. The findings indicate that the d-orbitals of both Mg and N atoms exhibit minimal contributions to the TDOS.

Elastic properties

The evaluation of elastic anisotropy is essential for comprehending the directional dependence of elastic

Table 1: Lattice parameter, band gap, of α-Mg3N2 following structural relaxation. Previously reported results are presented for comparison.

α-Mg_3N_2				
	Band gap	**Lattice Constant**	**Bulk Modulus (B_0)**	**Pressure derivative (B_0')**
Present work	1.728	9.9485	121.7	3.8
Reported data	2.8 [33], 1.45 [34], 1.63 [35]	9.952 [31]	110.7 [31]	4.0 [31]
Optimized atomic position				
Atom	x	y	z	
Mg	0.38	0.15	0.38	
N1	0.25	0.25	0.25	
N2	0.96	0.00	0.25	

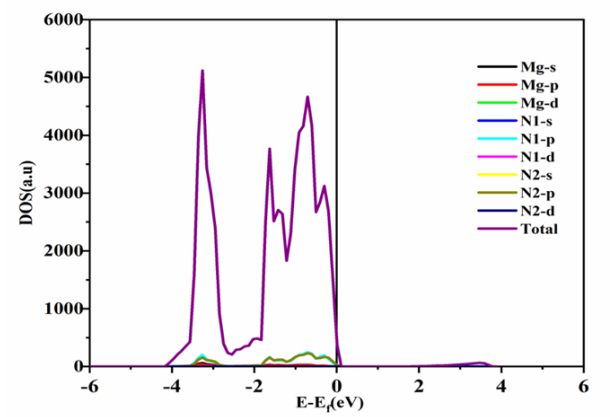

(a)

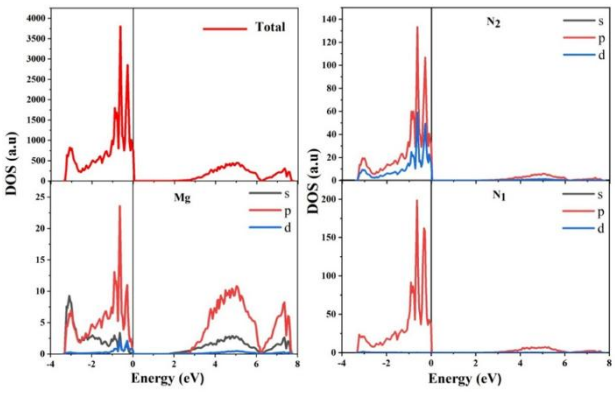

(b)

Figure 4: (a) Total and **(b)** site-specific DOS derived using the LCAO method for α-Mg_3N_2.

deformation in crystalline materials. This analysis plays a momentous role in the design and optimization of engineering devices. Assessing the elastic characteristics of Mg_3N_2 is vital for determining its structural integrity and mechanical rigidity. Table 2 presents the calculated elastic constants and moduli, providing insights into these characteristics. The determination of elastic constants that meet the Born stability criteria is essential for verifying the mechanical strength of a cubic crystal structure [36]. The Born stability requirements for the stability of a cubic structure is satisfied by the elastic constants are expressed mathematically as:

$$c_{11} + 2c_{12} > 0 \quad (1)$$

$$c_{44} > 0 \quad (2)$$

$$c_{11} - c_{12} > 0 \quad (3)$$

The resistance degree along the principal crystallographic direction is explained by the constant C_{11} .i.e., [100]. A measurement of shear deformation is provided by the elastic constant C_{44}. As Table 2 becomes evident, $C_{11} > C_{44}$ by 57.5%. There has been unidirectional distortion of the crystal structure. Moreover, when comparing the bulk's magnitude to the shear modulus, the parameter limiting mechanical stability in this combination is found to be the shear modulus. Young's modulus (E) is another parameter that determines the stiffness of the compound. The large value of E = 201.660 GPa indicates thatα-Mg_3N_2 is hard and ductile. Poisson's ratio (υ) is another way to measure a material's machinability. Poisson's ratio demonstrates how stable a compound is against shear. A value of υ = 0.225 indicates that the α-Mg_3N_2 crystal structure exhibits shear instability.

Table 2: Computed elastic components, bulk (B), Young's (E) and shear modulus (G), along with Poisson's ratio (υ) of α-Mg_3N_2 utilizing the Voigt- Reuss Hill's approach with PBE exchange-correlation functional.

Elastic Constants	**Findings (GPa)**	**Elastic Property**	**Findings (GPa)**
C_{11}	215.146	**B**	122.240
C_{12}	72.891	**G**	81.830
C_{44}	91.369	**E**	201.660
		υ	0.225 (Unit less)

Elastic Anisotropy

The level of elastic anisotropy varies across all natural materials. This study aims to comprehensively analyse the elastic anisotropy of the Mg_3N_2structure, by employing the Voigt and Reuss elastic moduli. We calculated the anisotropy indices for the bulk (A_B) and shear modulus (A_G), with the universal anisotropy index A^U, and the Zener

anisotropy factor A^Z using the respective mathematical formulations [36, 37]. The calculated values of A_B, A_G, A^U, and A^Zindicate that Mg_3N_2 exhibits pronounced shear anisotropy alongside nearly isotropic elastic compressibility.

$$A_B = \frac{B_V - B_R}{B_V + B_R} \quad (4)$$

$$A_G = \frac{G_V - G_R}{G_V + G_R} \quad (5)$$

$$A^U = \frac{B_V}{B_R} + 5\frac{G_V}{G_R} - 6 \quad (6)$$

$$A^Z = \frac{2C_{44}}{C_{11} - C_{12}} \quad (7)$$

All the nonzero values of the anisotropy parameters confirm the existence of finite anisotropy in Mg_3N_2 crystals. In contrast, for isotropic materials, the anisotropy parameters A_B, A_G, A^U are identically zero. If a solid appears, A_B, A_G, A^U, and A^Z of Mg_3N_2 0%, 0.82%, 0.05 and 1.3, respectively.

Table 3: Variations of Young's (E) and shear modulus (G)[in GPa], Poisson's ratio ν (unitless) and linear compressibilityβ[in $(TPa)^{-1}$] of Mg_3N_2.

	E_{Min}	E_{Max}	β_{min}	β_{max}	G_{Min}	G_{Max}	υ_{Min}	υ_{Max}
Present work[a]	178.250	218.730	2.771	2.771	71.128	91.369	0.133	0.294

[a]These values of G, E, β, ν have been calculated through ELATE software [32, 33].

Further, the different environmental arrangements of Mg-N_1 (N_2) atoms are taken into consideration while determining the directional characteristic of elastic moduli. Elastic moduli's angular fluctuation in three-dimensional (3D) space is seen in the fig. 5. Figure 5(b) displays a spherical model with linear compressibility in all directions, indicting zero anisotropy. (Fig. 5(a, c, and d)) show a model that is not spherical and has a significant amount of anisotropy. In the [001] direction, the shear modulus is found to reach its maximum value of 91.369 GPa, whereas Young's modulus is seen to increase in the same direction, reaching a minimum value of 178.250 GPa. The **directional dependence of Young's modulus** is a critical aspect of understanding the mechanical performance of crystalline materials, particularly anisotropic materials.

Young's modulus describes the stiffness of a material, and its directional dependence reflects how the material responds to stress differently depending on the crystallographic orientation. For example, in cubic crystals like iron or aluminium, Young's modulus is typically higher

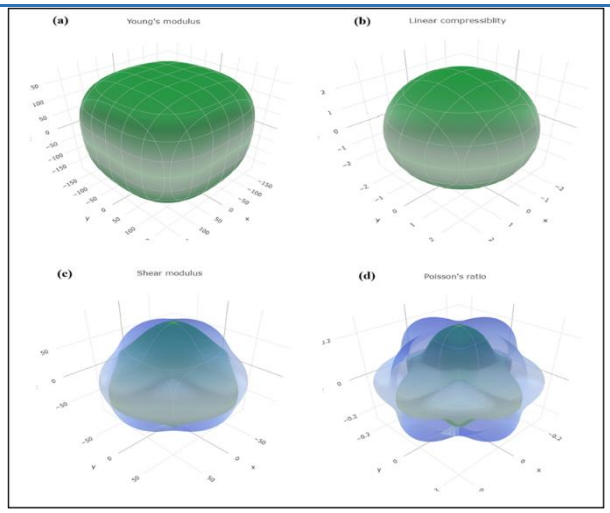

Figure 5: Angular variation of elastic modulus in 3-dimensional:(a) Young's modulus (b)linear compressibility, (c) shear modulus(d) Poisson's ratio for α-Mg_3N_2.

along the <111> direction compared to the <100> direction because atomic bonds are stronger and more densely packed along certain axes. In highly anisotropic materials like graphite or titanium alloys, this variation can be even more pronounced, with Young's modulus differing significantly between directions. This directional dependence directly impacts mechanical performance, as materials will exhibit different stiffness, deformation resistance, and stress-strain responses depending on the loading direction. For instance, in applications like aerospace components or biomedical implants, where materials are subjected to multidirectional stresses, understanding and optimizing the directional dependence of Young's modulus is crucial to prevent failure, ensure durability, and tailor materials for specific mechanical requirements. This anisotropy can significantly influence mechanical behaviour, including deformation, fracture, and load-bearing capacity. The extremes of these moduli suggest that because the material is less stiff along the [001] direction than along other directions, plastic deformation is more challenging to sustain along this direction.

Conclusion

The structural, mechanical, and electronic characteristics of the α-Mg_3N_2 material have been systematically explored using the GGA approach within the DFT framework. The optimized structural parameters were determined to characterize the material's structural attributes comprehensively. These structural data were subsequently employed to evaluate the electronic and mechanical properties of the compound. The results reveal that α-Mg_3N_2 exhibits semiconducting behaviour, exhibiting a calculated energy gap of 1.72 eV based on its electronic properties. The semiconducting nature of, α-Mg_3N_2 with a bang gap in the IR-Vis range is shown by its electronic band structure and density of states. This makes the compound

appropriate for use in both PV devices and infrared sensors. A detailed examination of the elastic attributes, like bulk, shear, Young's modulus, along with Poisson's ratio, is conducted. The analysis confirms that α-Mg_3N_2 possesses distinct elastic anisotropy. Specifically, the variation in Young's modulus ranges from a lowest amount of 178.250 GPa to a maximum value 218.730 GPa. While the shear modulus varies from a minimum of 71.128 GPa to its maximum value 91.369 GPa. The anisotropic elastic behaviour of α-Mg_3N_2 provides insights into the preferential crystallographic orientations, according to the elastic calculations, α-$Mg_3N_2$is a strong and ductile substance that can endure harsh environmental conditions while maintaining its ground state characteristics. The α-Mg_3N_2 efficiently used as a green energy source.

References

1. S. R. Römer, T. Doerfler, P. Kroll, and W. Schnick, Phys. Stat. solidi (b) 246: 1604-1613 (2009). https://doi.org/10.1002/pssb.200945011.
2. J. K. Jian, G. Wang, C. Wang, W. X. Yuan, and X. L. Chen, J. crys. Growth 291: 72-76, (2006), https://doi.org/10.1016/j.jcrysgro.2006.03.016.
3. Y. Zhuang, F. Sun, L. Zhou, C. Jiang, J. Wang, S. Li, and S. Liao, Int. J. App. Cer. Tech. 21: 2273-2287 (2024), https://doi.org/10.1111/ijac.14665.
4. L. Govindasamy, Y. J. Park, J. W. Ko, J. W. Lee, M. H. Jin, K. Kumar, and H. N. Kim, J. Korean Cer. Soc. 61: 507-536 (2024), https://doi.org/10.1007/s43207-024-00388-8.
5. A. E. Naclerio and P. R. Kidambi, Adv. Mater. 35: 2207374 (2023), https://doi.org/10.1002/adma.202207374.
6. N. Sorbie, Synthesis and structure of group I and II nitrides as potential hydrogen stores, PhD diss., University of Glasgow, 2011.
7. M. Leroux, N. Grandjean, J. Massies, B. Gil, P. Lefebvre, P. Bigenwald, and B. Gil, Phys. Rev. B 60: 1496 (1999), https://doi.org/10.1103/PhysRevB.60.1496.
8. V. Y. Davydov, A. A. Klochikhin, V. V. Emtsev, D. A. Kurdyukov, S. V. Ivanov, V. A. Vekshin, F. Bechstedt, J. Furthmüller, J. Aderhold, J. Graul, A. V. Mudryi, H. Harima, A. Hashimoto, A. Yamamoto, and E. E. Haller, Phys. Stat. Solidi (b), 234: 787-795 (2002), https://doi.org/10.1002/1521-3951(200212)234:3<787::AID-PSSB787>3.0.CO;2-H.
9. V. Y. Davydov, A. A. Klochikhin, V. V. Emtsev, A. N. Smirnov, I. N. Goncharuk, A. V. Sakharov, D. A. Kurdyukov, M. V. Baidakova, V. A. Vekshin, S. V. Ivanov, J. Aderhold, J. Graul, A. Hashimoto, and A. Yamamoto, Phys. Stat. Solidi (b), 240: 425-428 (2003), https://doi.org/10.1002/pssb.200303448.
10. D. E. Partin, D. J. Williams, and M. O'Keeffe, J. solid state chem., 132: 56-59, (1997), https://doi.org/10.1006/jssc.1997.7407.
11. O. Reckeweg and F. J. DiSalvo, Zeitschrift für anorganische und allgemeine Chemie 627, 371-377, (2001), https://doi.org/10.1002/1521-3749(200103)627:3<371::AID-ZAAC371>3.0.CO;2-A.
12. A. M. Nartowski, and I. P. Parkin, Polyhedron 21: 187-191, (2002), https://doi.org/10.1016/S0277-5387(01)00974-3.
13. H. Z. Ye, X. Y. Liu, and B. Luan, Mater. letters, 58: 2361-2364 (2004), https://doi.org/10.1016/j.matlet.2004.02.028.
14. J. Cui, D. Meng, Z. Wu, W. Qin, D. She, J. Kang, R. Zhang, C. Wang, and W. Yue, Cer. International 48: 363-372 (2022), https://doi.org/10.1016/j.ceramint.2021.09.111.
15. M. Ullah, S. Khan, A. Laref, and G. Murtaza, Philos. Mag. 100: 768-781, (2020), https://doi.org/10.1080/14786435.2019.1697835.
16. U. Paliwal, and K. B. Joshi, J. Phys. D: Appl. Phys 44: 255501(1-7), (2011). https://doi.org/10.1088/0022-3727/44/25/255501.
17. S. R. Römer, T. Dörfler, P. Kroll, and W. Schnick, Phys. Status Solidi B 246, 1604–1613, (2009). https://doi.org/10.1002/pssb.200945011.
18. S. R. Römer, W. Schnick, and P. Kroll, J. Phys. Chem. C. 113: 2943-2949, (2009), https://doi.org/10.1021/jp8077002.
19. C. Braun, S. L. Börger, T. D. Boyko, G. Miehe, H. Ehrenberg, P. Höhn, and W. Schnick, J. Am. Chem. Soc. 133: 4307-4315, (2011), https://doi.org/10.1021/ja106459e.
20. A. Mokhtari, and H. Akbarzadeh, Phys. B Cond. Mat. 337, 122-129, (2003), https://doi.org/10.1016/S0921-4526(03)00387-9.
21. E. Orhan, E. Jobic, R. Brec, R. Marchand, and J. Y Saillard, J. Mater. Chem. 12: 2475-2479, (2002). https://doi.org/10.1039/B203500F.
22. R. Dovesi, A. Erba, R. Orlando, C. M. Zicovich-Wilson, B.Civalleri, L. Maschio, M. Rérat, S. Casassa, J. Baima, S. Salustroand and B. Kirtman, WIREs Comput. Mol. Sci. 8, (2018). https://doi.org/10.1002/wcms.1360.
23. R. Dovesi, V. R. Saunders, C. Roetti, R. Orlando, C. M. Zicovich-Wilson, F. Pascale, B. Civalleri, K. Doll, N. M. Harrison, I. J. Bush, P. D'Arco, M. Llunell, M. Causà, Y. Noël, L. Maschio, A. Erba, M. Rérat and S. Casassa 2017 CRYSTAL17 User's Manual (University of Torino).
24. M. F. Peintinger, D. V. Oliveira, T. Bredow, J. Comput. Chem. 34: 451-459 (2013), https://doi.org/10.1002/jcc.23153.
25. D. V. Oliveira, M. F. Peintinger, J. Laun, T. Bredow,

J. Comput. Chem. 40: 2364-2376, (2019), https://doi.org/10.1002/jcc.26013.
26. J. P. Perdew, K. Burke, M. Ernzerhof, Phys. Rev. Lett. 77: 386, (1996), https://doi.org/10.1103/PhysRevLett.77.3865.
27. J. P. Perdew, A. Ruzsinszky, G. I. Csonka,O. A. Vydrov, G. E. Scuseria, L. A. Constantin, X. Zhouand K. Burke, Phys. Rev. Lett. 100: 136406 (2008), https://doi.org/10.1103/PhysRevLett.100.136406.
28. H. J. Monkhorst, J. D. Pack, Phys. Rev. B 13: 5188-92, (1976), https://doi.org/10.1103/PhysRevB.13.5188.
29. C. G. Broyden, Math. Comput., 19, 577-93, (1965), https://doi.org/10.2307/2003941.
30. D. D. Johnson, Phys. Rev. B 38: 12807-13, (1988), https://doi.org/10.1103/PhysRevB.38.12807.
31. J. Hao, Y. Li,Q. Zhou,D. Liu, M. Li, F. Li,X, and Li X, Inorg. Chem. 48: 9737-9740, (2009), https://doi.org/10.1021/ic901324n.
32. A. Erba, A. Mahmoud, D. Belmonte, R. Dovesi, J. Chem. Phys. 140: 124703, (2014), https://doi.org/10.1063/1.4869144.
33. K. Toyoura, T. Goto, K. Hachiya, and R. Hagiwara, Electrochimicaacta, 51: 56-60, (2005), https://doi.org/10.1016/j.electacta.2005.04.004.
34. E. Orhan, S. Jobic, R. Brec, R. Marchand, J. Y. Saillard, J. Mater. Chem. 12: 2475-2479 (2002), https://doi.org/10.1039/B203500F.
35. J. Li, C. Fan, X. Dong, Y. Jin, and J. He, J. Phys. Chem. C, 118: 10238-10247 (2014), https://doi.org/10.1021/jp411692n.
36. J. Gao, Q. J. Liu, and B. Tang, J. App. Phys., 133: 135901 (2023), https://doi.org/10.1063/5.0139232.
37. R. Gaillac, P. Pullumbi, and F. X. Coudert, J. Phys.: Condens. Matter, 28: 275201, (2016), https://doi.org/10.1088/0953-8984/28/27/275201.